



Geochemistry, petrogenesis and petrology of intrusive rocks in Shadan gold deposit, SW Birjand, Eastern Iran

Parinaz Yazdi^{ID}, Ali Kananian *^{ID}, Davood Raeisi^{ID}, Soroush Modabberi^{ID}

School of Geology, College of Sciences, University of Tehran, Tehran, Iran

Received: 13 August 2022, Revised: 19 October 2022, Accepted: 24 October 2022

© University of Tehran

Abstract

Shadan gold (+copper) deposit in the Lut block, east of Iran, comprises Eocene to Oligocene intrusive and subvolcanic rocks with intermediate to felsic composition, which have intruded into Eocene volcanic-pyroclastic rocks. Shadan intrusive rocks range from granodiorite, quartz monzonite, and diorite to microgabbrodiorite. Geochemical data indicate that Shadan intrusive rocks are I-type, metaluminous to peraluminous, belonging to the calc-alkaline to high-potassic calc-alkaline magmatic series. Rare earth elements (REE) and trace elements patterns of Shadan rocks display enrichment in light rare earth elements (LREE) and large ion lithophile elements (LILE) relative to heavy rare earth elements (HREE) and high field strength elements (HFSE). The main hydrothermal alteration types contain quartz-carbonate, propylitic, argillic, phyllic and potassic, which affected the rocks in varying degrees. According to tectonomagmatic discrimination diagrams, all rock samples display evidence of a volcanic arc, which was formed at an active continental margin. Based on Nb/Y vs. Rb/Y ratio, Shadan rock samples experienced subduction zone enrichment and crustal contamination. According to Nb/Zr vs. Nb/Ba ratio, source region of the Shadan intrusive and subvolcanic rocks are attributed to the subcontinental lithosphere source. Th/Yb versus Nb/Yb diagram shows a separation between Shadan samples and MORB-OIB arrays, possibly due to crustal contamination and the mobility of Th during subduction. La vs. La/Yb ratio reveals that partial melting played a significant role in the formation of Shadan rocks.

Keywords: Shadan Gold Deposit, Porphyry Deposit, Petrogenesis, Crustal Contamination, Lut Block.

Introduction

Iran is located in the central part of the Tethyan orogenic and metallogenic belt, and its diversity in magmatism, geodynamics and mineralization is a consequence of the subduction of various generations of Tethyan Ocean and the accretion of Gondwana-derived micro-continents to the southern margin of Eurasia (Stocklin, 1968; Berberian & King, 1981; Richards & Sholeh, 2016). Numerous mineral deposits are known to be associated with the Neotethyan Ocean evolution (Richards, 2015). This subduction and subsequent collision have produced three main magmatic belts: (i) the Eastern Iranian Magmatic Belt (EIMB), (ii) Urumieh-Dokhtar Magmatic Belt (UDMB), and (iii) the Alborz-Azerbaijan Magmatic Belt (AAMB) (Berberian & King, 1981; Verdel et al., 2011; Pang et al., 2013; Omidianfar et al., 2020).

The Sistan suture zone is a branch of the Neotethyan Ocean with a complex tectonic history (Camp & Griffis, 1982; Tirrul et al., 1983; Pang et al., 2013). Magmatic activity in Sistan suture zone and generally in east of Iran was occurred during a period mostly from Middle Eocene to the Late Oligocene (Pang et al., 2013). Subduction between the Lut Block and the Afghan Block is a controversial issue and various tectono- magmatic theories have been proposed. Verdel et al. (2011) ascribed the mineralization in the Eastern Iran to an extensional rift basin but most

* Corresponding author e-mail: kananian@ut.ac.ir

researchers believe that the subduction is an undeniable subject. Saccani et al. (2010) by studying the ophiolitic complex of Nehbandan, suggested that subduction has played a key role in closure of the Sistan Ocean and the associated mineralization, resulted from the eastward intra-oceanic subduction of the Sistan Ocean beneath the Afghan Block. In addition, Camp & Griffis (1982) and Tirrul et al. (1983) proposed that magmatic activity in East of Iran resulted from eastward subduction of the Sistan Ocean beneath the Afghan Block. On the other hand, Berberian & King (1981), Zarrinkoub et al. (2012) and Pang et al. (2013) proposed that subduction of the Sistan ocean was westward beneath the Lut Block. Meanwhile, two-sided asymmetric subduction is another theory in closure of the Sistan Ocean (Arjmandzadeh et al., 2011). Omidianfar et al. (2020) studied the Koudakan intrusive in EIMB, and proposed a delamination of thickened lithosphere after collision between the Lut Block and Afghan Block.

The Tertiary plutonic and volcanic rocks are widely distributed in southwest of Birjand and recently, significant deposits have been reported in this area including Maherabad, Khopik, Khunic and Hired. Mahdavi et al. (2020) stated that the Shadan area is a porphyry deposit. Richards (2012) determined the age of the Shadan gold (+copper) deposit as 37.26 ± 0.26 Ma. Malekzadeh & Karimpour (2011) reported the U-Pb zircon ages of the 39 ± 0.8 Ma from monzonite rocks of the Maherabad Cu-Au deposit. Malekzadeh et al. (2014) attributed the formation of the Khopic porphyry copper deposit to Middle Eocene magmatism in eastern Iran. The Khunic area has been studied by Samiee et al. (2019) who believed that the hydrothermal breccia in the central part of the area is the main mineralization phase. As reported by Karimpour et al. (2007), the Hired gold-tin prospecting area is associated with S-type granites.

Due to the ambiguities about the petrogenesis of magmatic systems in Shadan area, the purpose of this study is to discuss and present the geochemical data to decipher the petrogenesis and petrology of the Shadan intrusive and subvolcanic rocks in the East of Iran in the context of geodynamics and metallogenic evolution of the system (Fig. 1).

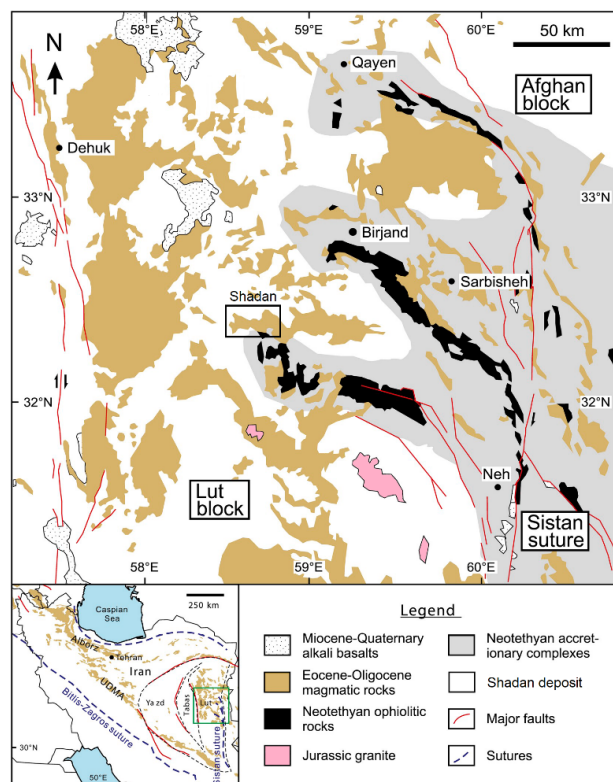


Figure 1. Geological map of Lut-Sistan region, east of Iran and location of the Shadan deposit in the Lut Block (Modified from Pang et al., 2013 and Modabberi et al., 2019)

Geological Setting

Shadan area is located in 60 km southwest of Birjand, near the Khouf town, in the Lut Block, ($32^{\circ}23'42''$ - $32^{\circ}20'56''$ N and $58^{\circ}56'96''$ - $58^{\circ}59'57''$ E) in the South Khorasan province, Iran. The Lut Block with a length of 900 km is one of the structural units of the Central Iran micro-continent, which is bounded to the west by the Nayband Fault, to the east by the Nehbandan fault and Sistan suture zone, to the north by the Dorouneh fault and to the south by the Jazmourian depression (Berberian & King, 1981). The Lut Block is composed of a pre-Jurassic metamorphic basement, Jurassic sedimentary rocks and various generation of Late Mesozoic and Cenozoic volcanic-intrusive rocks (Camp & Griffis, 1982; Tirrul et al., 1983). The magmatic activity in the Lut Block initiated in the middle Jurassic (165-162 Ma) and its peak was in the Tertiary (Karimpour et al., 2011). In terms of geological situation, Shadan gold (+copper) deposit is located in the 1:250000 Birjand geological map (Vahdati-Daneshmand & Eftekhar-Nejad, 1991) and in the northeast corner of the 1:100000 geological map of Sarcheh-e-Shoor (Vassigh & Soheyli, 1975).

Based on the 1:100000 sheet of Sarcheh-e-Shoor, study area consists of dacite, altered andesite, tuff breccia and a number of subvolcanic to intrusive rocks. However, field evidence and petrographic studies indicated that most of the volcanic rocks in the Sarcheh-e-Shoor geological map, are subvolcanic and intrusive rocks. According to the 1:1000 Shadan geological map (Karand Sadr-e-Jahan Co. 2022) and field studies (Fig. 2), lithological units can be divided into three units:

1) Eocene volcanic-pyroclastic rocks with intermediate to mafic composition, which have undergone quartz-carbonate, argillic and propylitic alteration,

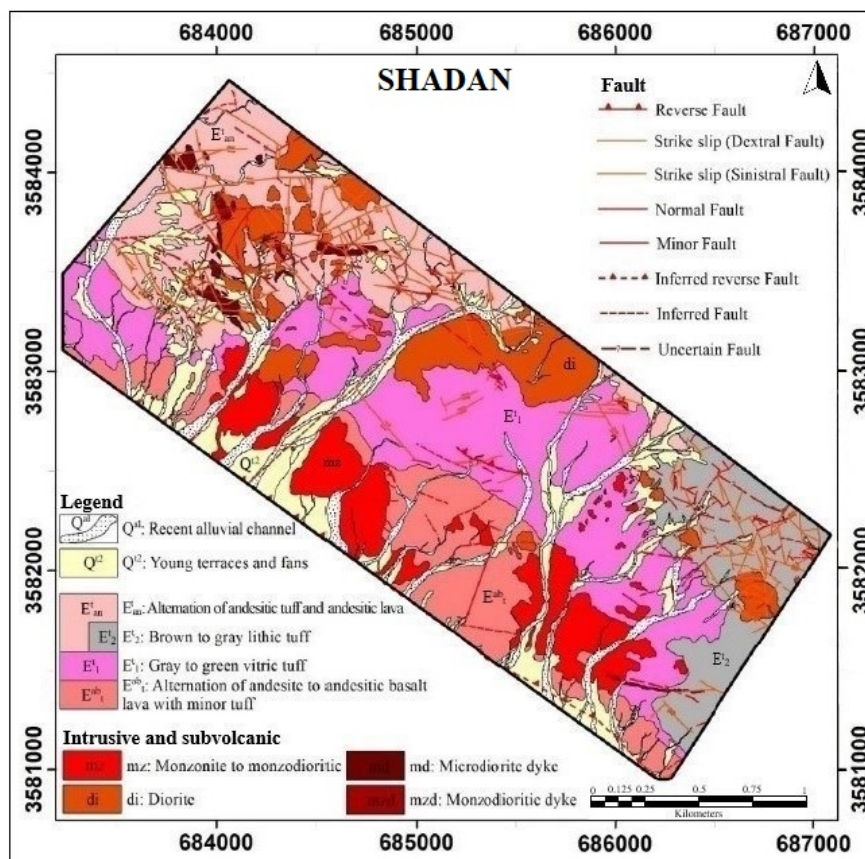


Figure 2. Simplified geological map of the Shadan area (Karand Sadr-e-Jahan Co. 2022)

2) Eocene-Oligocene subvolcanic and intrusive rocks with northwest-southeast trend and intermediate to felsic composition, which intruded into the volcanic-pyroclastic rocks. These rocks consist of granodiorite to gabbro-diorite with potassic, sericitic, argillic, quartz-carbonate and propylitic alteration,

3) Quaternary unit, consisting of young and old terraces, recent alluvium and debris.

Based on the tectonic studies, faults especially strike-slip faults are major structures in the Shadan area. Approximately, faults have been formed in all directions in the study area; however, most of the faults have east-west and northwest-southeast trends.

Materials and methods

More than 100 samples were collected from the Shadan area for petrographical and geochemical studies. 80 thin sections were prepared from surface and fresh samples at University of Tehran for microscopic study. From these samples, 11 least altered samples were selected for geochemical analyses. The major elements of Shadan rock samples were analyzed by Inductively Coupled Plasma-Optical Emission Spectrometry (ICP-OES), using Agilent 735. Trace elements and rare earth elements were determined by Inductively Coupled Plasma-Mass Spectrometry (ICP-MS) following lithium metaborate fusion and digested by nitric acid, using Perkin Elmer DRC-e 9000 at Zarazma Laboratory, Iran. Data were interpreted using GCDkit and Microsoft Excel software.

Petrography

Intrusive and subvolcanic rocks in the Shadan area intruded into the Eocene-Oligocene volcanic-pyroclastic units. The composition of these rocks is granodiorite porphyroid to micro-gabbrodiorite porphyroid. Most of these rocks have porphyroid textures with 30 % to 70 % phenocrysts including plagioclase, K-feldspar, hornblende and biotite (Fig. 3a). The phenocrysts set in a fine to medium grained groundmass. Intrusive and subvolcanic units in the study area can be divided to four units as follows:

Granodiorite

The granodiorites display porphyroid texture with medium-grained groundmass and 45 vol % of phenocrysts. The phenocrysts mostly consist of euhedral-subhedral plagioclase (45-66 vol %), K-feldspar (13-23 vol %), quartz (22-42 vol %), hornblende (4-9 vol %) and biotite (3-11 vol %). The rock matrix is mainly plagioclase, K-feldspar, quartz and opaque minerals (Fig. 3b).

Quartz monzonite

These rocks have porphyroid texture and phenocrysts set in medium-grained groundmass of mostly plagioclase, K-feldspar, quartz, opaque minerals and traces of apatite. The phenocrysts comprise 41-47 vol % plagioclase, 24-27 vol % K-feldspar and 15-17 vol % quartz (Fig. 3c).

Diorite

The diorites have porphyroid texture with fine-grained groundmass consisting of plagioclase, K-feldspar, quartz and opaque minerals. Phenocrysts include 42-58 vol% euhedral to subhedral plagioclase, 9-12 vol % K-feldspar, 13-19 vol % quartz and 9-11 vol% hornblende (Fig. 3d).

Microgabbrodiorite

The microgabbrodiorite dykes indicate porphyroid texture with fine-grained groundmass mostly consist of plagioclase, hornblende, K-feldspar, quartz, apatite and opaque minerals. Phenocrysts include of 48-62 vol % plagioclase, 11-16 vol % hornblende, 10-12 vol % K-feldspar and 6-9 vol % quartz (Fig. 3e and f).

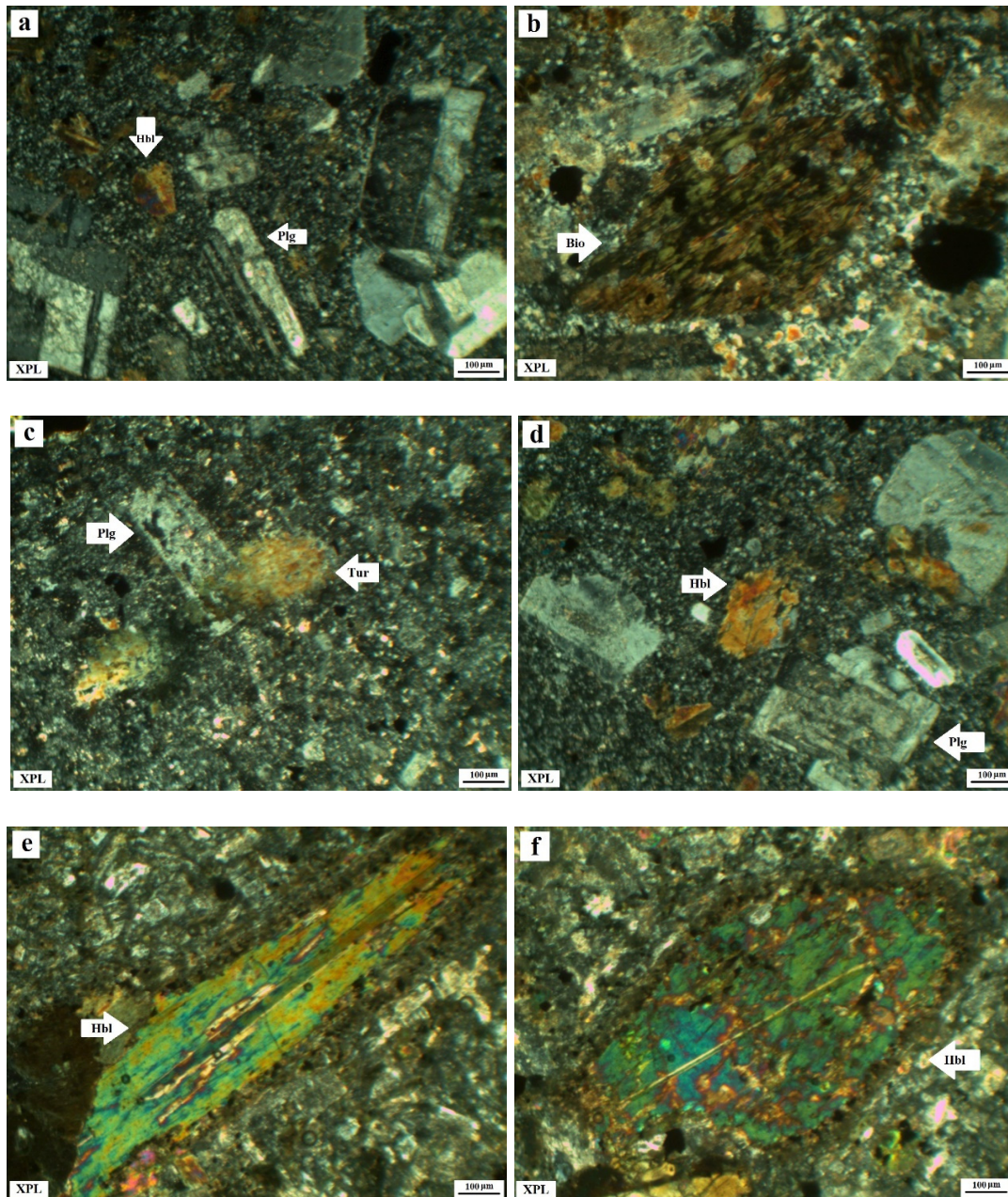


Figure 3. The main minerals and porphyroid texture in the rock sequence of the Shadan area. a) porphyroid texture in diorite; b) biotite (Bio) in granodiorite; c) plagioclase (Plg) and tourmaline (Tur) in quartz monzonite; d) plagioclase and hornblende (Hbl) in diorite; e and f) hornblende in microgabbrodiorite

Alteration

The field, petrography and previous reports of the Shadan deposit exploration operations indicate that all lithological units in the study area have been affected by various alteration styles. Hydrothermal alterations in the Shadan area include quartz-carbonate, propylitic, argillic, phyllic and potassic. (Fig. 4).

Quartz-carbonate alteration affects all rock types occurred along faults and fractures and can be divided into two silicic and carbonate alterations based on the abundance of the minerals formed. This alteration is associated with gold mineralization. Quartz-carbonate alteration mainly consist of quartz, calcite and lesser amounts of sericite. Quartz and calcite are represented as vein, veinlets and in groundmass of rocks. This alteration is distinguished by red color on the surface of the area. Some of plagioclases has been replaced by calcite in quartz-carbonate alteration zones (Fig. 5a).

Propylitic alteration occurs in the margin of the Shadan porphyry system, especially in the southeast, north and northeast of the area. It is characterized by green color on the surface, and it mainly has affected volcanic and pyroclastic units. The intrusive rocks were not affected severely by this type of alteration. This alteration is distinguished by chlorite, epidote, calcite, sericite and lesser amounts of quartz. These minerals were formed through the alteration of mafic minerals and plagioclase. Mineralization in this alteration is limited (Fig. 5b).

Argillic alteration is the most extensive alteration in the Shadan area, which includes kaolinite, montmorillonite and calcite formed by the acid leaching of primary minerals such as feldspars. Mineralization has been occurs as stockwork and disseminated (Fig. 5c and d). Phyllic alteration has limited extent and affected quartz monzonite rocks in the Shadan area. This alteration is characterized by sericite, quartz, calcite, chlorite and opaque minerals. Phyllic alteration is gradually changes to argillic alteration in the surface, and mineralization in this zone is intense (Fig. 5e). Tourmalinization occurs locally in areas affected by phyllic alteration. It is identified by replacement of primary minerals by tourmaline in the last stage of hydrothermal alteration (Fig. 5f).

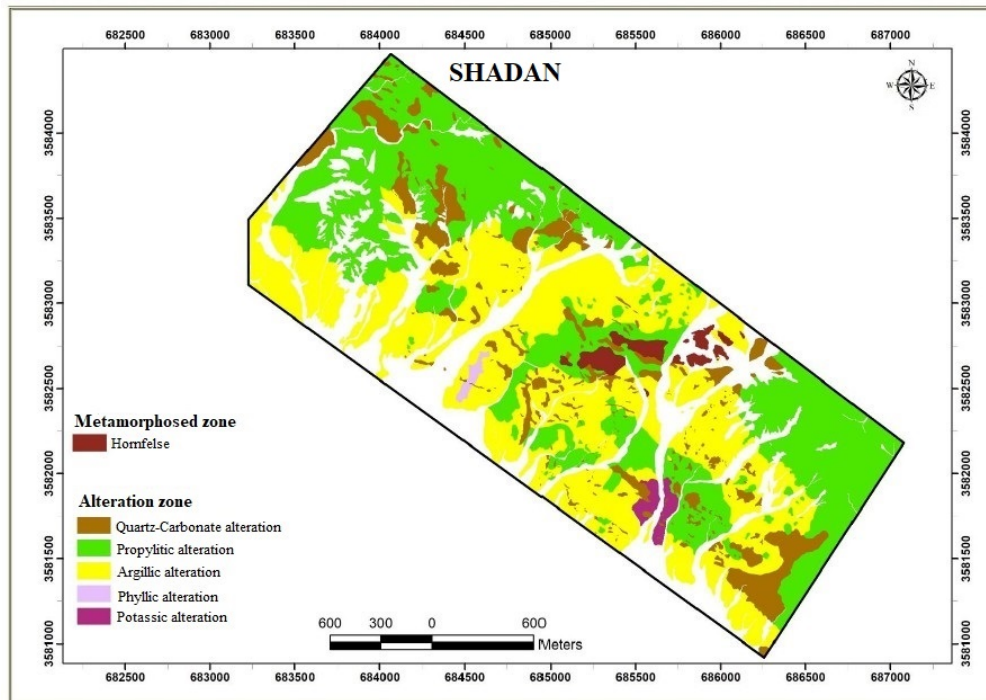


Figure 4. Alteration map of the Shadan area

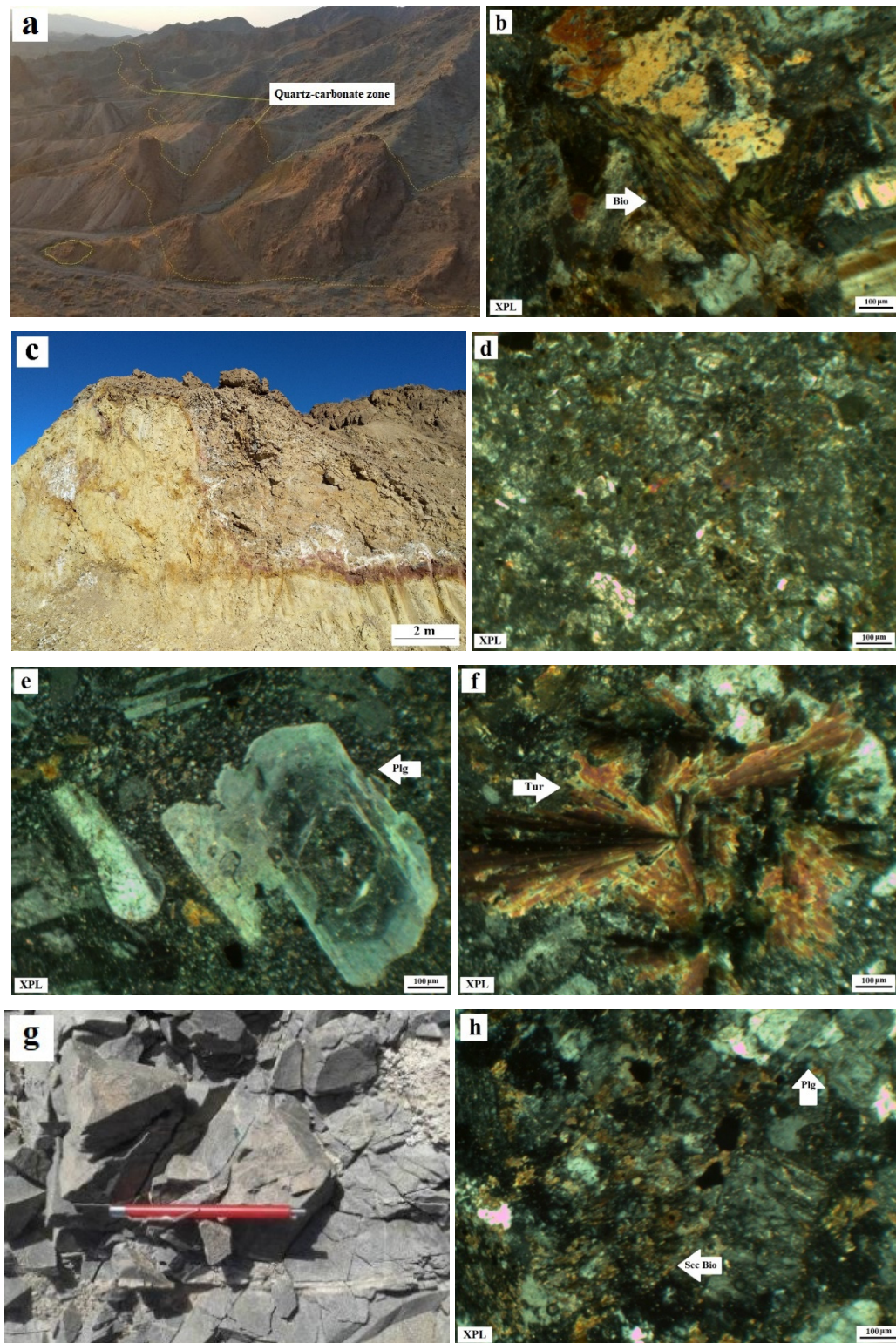


Figure 5. Field photographs and photomicrographs of hydrothermal alteration: a) quartz-carbonate alteration zone, b) replacement of biotite by chlorite in propylitic zone, c and d) argillic zone, e) replacement of plagioclase by sericite in phyllic zone, f) tourmaline and g) field photograph of potassic alteration in quartz monzonite and h) formation of secondary biotite (Sec Bio) in quartz monzonite due to potassic alteration

Potassic alteration has temporal-spatial relationship with Shadan intrusive rocks. Potassic alteration minerals consists of secondary biotite and K-feldspar (Fig. 5g and h).

Geochemistry of Shadan intrusive rocks

The major, trace and rare earth elements geochemical analyses results for Shadan area are presented in Table 1. The Shadan intrusive rocks have a range of SiO₂ contents from 54.11 to 68.11 wt. %. In the Na₂O+K₂O vs. SiO₂ diagram (Middlemost, 1994), rock samples plot within the fields of granodiorite, diorite, quartz monzonite and gabbrodiorite (Fig. 6a). In the A/CNK versus A/NK diagram (Shand, 1943), Shadan rock samples fall in the fields of metaluminous and peraluminous (Fig. 6b). The AFM (Na₂O+K₂O, FeO total and MgO) diagram (Irvine & Baragar, 1971) presents that the rock samples have calc-alkaline series trend. (Fig. 6c). In the diagram of K₂O vs. SiO₂, (Peccerillo & Taylor, 1976), rock samples mainly plot in the calc-alkaline series field, some samples show a trend in the high-K calc-alkaline series, except for one sample which plots within the Shoshonite series (Fig. 6d). The Shadan intrusive rocks plot within the I-type granitoids field in the K₂O versus Na₂O diagram (Chappell & White, 2001) (Fig. 6e).

Table 1. Concentration of major oxides (in wt. %) and trace elements (in ppm) in the analyzed Shadan rocks samples

Rock type Sample	Gabbrodiorite		Quartz monzonite		Diorite			Granodiorite			
	99-I-05	99-I-03	99-I-15	99-I-13	99-I-10	99-I-17	99-I-19	99-I-08	99-I-09	99-I-20	99-I-21
SiO ₂	54.24	54.11	62.66	62.06	60.87	61.51	58.39	63.13	68.11	63.37	63.11
Al ₂ O ₃	16.98	16.82	16.9	16.71	17.95	17.03	13.02	17.98	15.96	16.72	17.69
BaO	<0.01	<0.01	0.07	0.07	<0.01	0.05	<0.01	<0.01	0.06	<0.01	<0.01
CaO	7.31	6.38	2.07	1.39	3.92	5.44	5.7	2.57	0.93	4.55	3.64
Fe ₂ O _{3(T)}	8.67	8.61	5.63	5.27	6.49	5.59	6.6	7.02	3.8	4.12	4.92
Fe ₂ O ₃	2.85	3.04	2.45	2.33	2.35	2.00	2.24	2.57	1.51	1.62	1.88
FeO _(T)	7.79	7.74	5.06	4.73	5.83	5.02	5.93	6.31	3.41	3.70	4.42
FeO	5.19	4.97	2.83	2.61	3.69	3.20	3.88	3.97	2.03	2.22	2.71
K ₂ O	1.92	2.04	3.63	3.99	1.96	1.87	2.26	1.42	3.48	1.59	1.98
MgO	4.59	4.51	1.77	2.24	2.47	2.57	8.71	2.61	1.48	2.51	1.8
MnO	0.23	0.21	<0.01	<0.01	0.06	0.08	0.08	0.07	<	0.05	<
Na ₂ O	2.76	3.55	4.53	4.45	3.58	3.45	2.6	4.11	2.96	5.01	4.15
P ₂ O ₅	0.3	0.31	0.28	0.28	0.2	0.27	0.1	0.31	0.12	0.27	0.17
TiO ₂	0.63	0.64	0.49	0.47	0.49	0.46	0.71	0.64	0.34	0.48	0.39
LOI	2.18	2.53	1.97	2.78	1.89	1.53	1.71	3.06	2.46	1.25	2.15
Ag	<0.1	0.1	<0.1	<0.1	<0.1	<0.1	<0.1	<0.1	<0.1	0.1	0.1
Al	79660	88669	88339	80505	86398	59891	77896	77771	62347	91464	93542
As	21.4	34.1	16	8	6.5	7.5	7.7	11.3	1.6	17.7	7
Ba	486	450	858	815	510	510	92	243	590	537	421
Be	0.9	1	1.3	1.2	1.2	1	1	1.1	1.1	1.5	1.2
Bi	<0.1	<0.1	0.2	0.4	<0.1	<0.1	<0.1	<0.1	0.6	0.2	<0.1
Ca	46317	42870	13516	8143	25157	28204	41522	15205	4915	34301	26735
Cd	0.1	0.1	<0.1	<0.1	0.4	<0.1	<0.1	0.2	0.2	<0.1	<0.1
Ce	38	42	54	53	38	44	51	49	47	67	35
Co	23	26.3	19.7	25.4	16.7	7.4	32.6	39.6	22.1	8.2	7.8
Cr	85	71	25	27	21	16	523	27	8	27	12

Cs	4.3	1.4	12.3	6.6	15.2	2.7	16.6	4.5	5.5	2.9	6.4
Cu	25	158	96	162	23	12	28	151	1364	96	106
Dy	2.49	2.53	2.44	3.32	2.25	2.29	1.9	2.75	2.61	2.42	1.84
Er	1.4	1.5	1.33	1.61	1.16	1.21	1.09	1.37	1.32	1.32	1
Eu	1.52	1.58	2.54	3.05	1.49	1.58	0.39	1.23	2.2	1.85	1.35
Fe	57319	60335	41659	39925	48002	32526	46832	46846	25007	30890	39242
Gd	1.61	1.8	2.08	2.34	1.49	1.86	1.66	2.08	1.86	2.43	1.38
Hf	1.7	1.9	1.34	1.33	1.26	1.51	1.55	1.28	1.33	1.41	1.27
In	<0.5	<0.5	<0.5	<0.5	<0.5	<0.5	<0.5	<0.5	<0.5	<0.5	<0.5
K	17308	17794	29220	29212	16682	12599	21541	10666	23401	14685	18511
La	18	20	30	31	20	22	28	21	25	37	16
Li	30	25	17	18	24	17	24	17	15	7	21
Lu	0.19	0.2	0.16	0.21	0.18	0.14	0.14	0.19	0.21	0.16	0.16
Mg	>2%	>2%	11075	13177	14736	11993	>2%	14204	7687	14786	11468
Mn	1698	1372	200	218	524	508	588	557	212	372	290
Mo	<0.1	1	<0.1	<0.1	<0.1	<0.1	<0.1	<0.1	2	<0.1	<0.1
Na	18145	23911	28546	26468	23006	18531	19801	23636	15498	35990	29041
Nb	4.3	5	4.2	4.7	4	4.5	5.6	3.7	3.9	5.3	5
Nd	16.3	17.8	20.1	27	14.3	18.9	14.1	19.7	17.7	22.6	11.4
Ni	47	46	13	15	7	11	367	8	4	14	7
P	1147	1182	1176	1082	817	904	427	1195	386	1152	727
Pb	24	5	6	6	11	7	<1	18	17	3	<1
Pr	4.72	4.96	5.53	6.8	4.38	5.27	4.61	5.66	5.28	6.65	3.71
Rb	48	57	141	171	76	43	135	52	96	49	89
S	710	783	392	1265	464	316	1268	555	449	491	418
Sb	2	3.6	1.3	1.2	<0.5	1.3	1.1	4	0.7	1.8	0.7
Sc	22.1	23.7	11.5	11.3	12	10.1	19.4	10	6.4	10.3	7.4
Se	<0.5	<0.5	<0.5	<0.5	<0.5	<0.5	<0.5	<0.5	<0.5	<0.5	<0.5
Sm	2.41	2.59	4.68	6.46	2.07	3.03	<0.02	1.88	3.61	3.31	1.06
Sn	0.7	0.8	1.1	1.2	1.4	0.6	1.4	0.7	1.3	1.1	1.4
Sr	673.2	754.1	506.8	477.6	665.1	648	214.8	498.9	224.8	756.4	574.3
Ta	0.47	0.45	0.37	0.4	0.35	0.42	0.45	0.37	0.45	0.45	0.38
Tb	0.52	0.54	0.53	0.7	0.44	0.49	0.41	0.6	0.54	0.55	0.4
Te	0.64	1.31	2.5	0.97	1.01	1.33	<0.1	<0.1	1.52	0.71	0.95
Th	5.75	5.82	8.88	7.42	6.13	6.52	6.84	5.25	11.94	6.8	6.54
Ti	4042	4258	3348	3251	3195	2672	4738	3763	1591	3266	2890
Tl	0.15	0.33	0.67	0.84	0.98	0.24	0.97	0.76	1.05	0.11	0.51
Tm	0.26	0.22	0.19	0.21	0.17	0.16	0.17	0.19	0.22	0.16	0.17
U	0.9	1	1.4	1.4	0.8	1.1	0.5	0.6	1.7	1.6	1.1
V	249	266	160	152	187	118	150	171	102	152	136
W	<1	<1	<1	<1	<1	<1	<1	<1	<1	<1	1.4
Y	16.5	16.9	14.4	17.3	14.9	12.7	14.3	14.3	13.5	12.6	11.9
Yb	1.6	1.6	1.4	1.7	1.4	1.1	1.1	1.6	1.5	1.3	1.2
Zn	90	79	29	39	92	32	30	48	34	36	32
Zr	32	42	13	9	13	17	63	30	12	16	12
Eu/Eu*	0.75	0.71	0.75	0.69	0.83	0.64		0.62	0.80	0.64	1.10
K₂O/Na₂O	0.69	0.57	0.80	0.89	0.54	0.54	0.86	0.34	1.17	0.31	0.47
Mg#	0.34	0.34	0.23	0.29	0.27	0.31	0.56	0.27	0.28	0.37	0.26

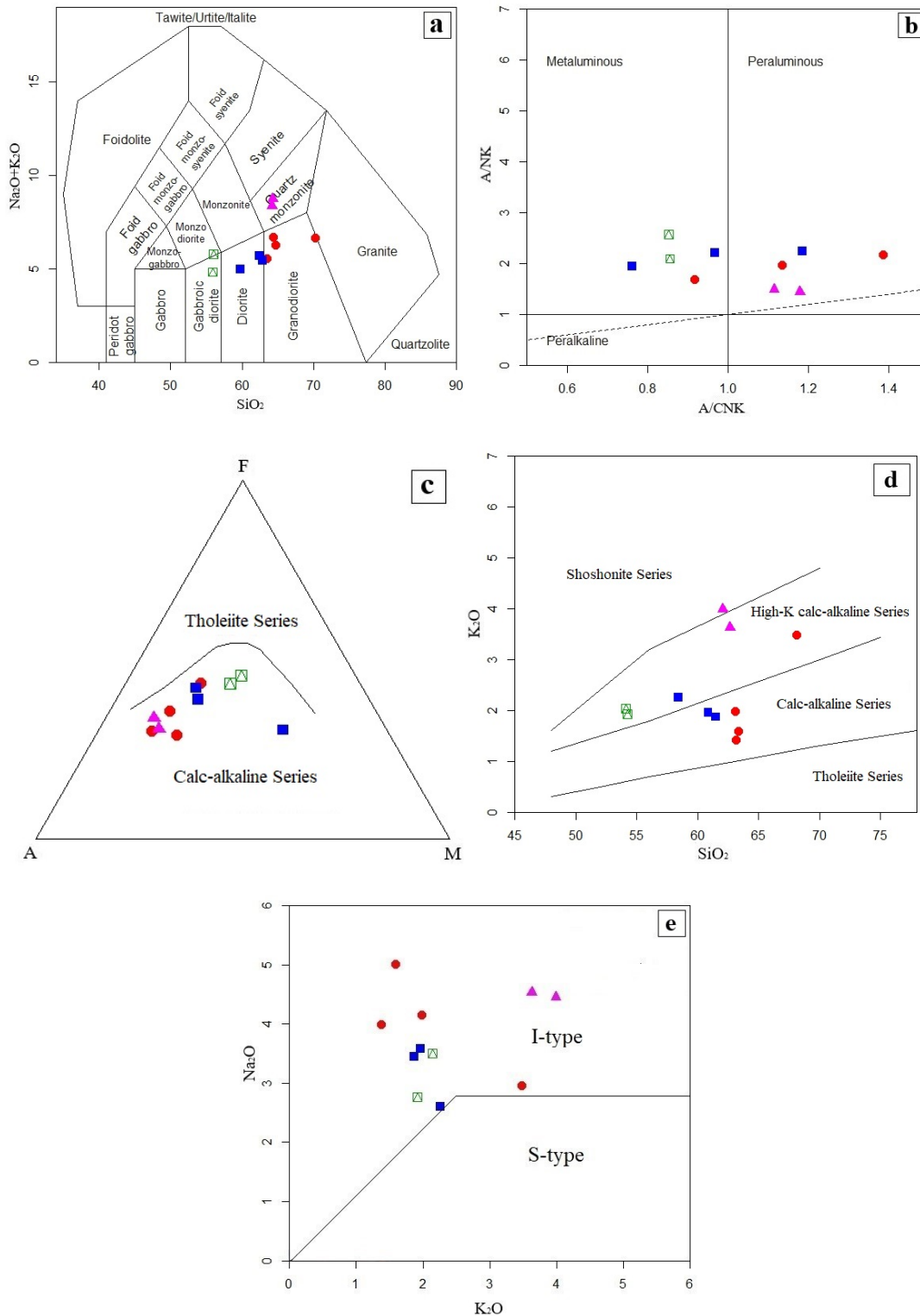


Figure 6. Geochemical classification diagrams: a) Na₂O+K₂O vs. SiO₂ diagram (Middlemost, 1994); b) Al₂O₃ / (CaO+K₂O+Na₂O) vs. Al₂O₃ / (Na₂O + K₂O) diagram (Shand, 1943); c) the AFM (Na₂O+K₂O, FeO total and MgO) diagram (Irvine & Baragar, 1971); d) K₂O vs. SiO₂ diagram (Peccerillo & Taylor, 1976); e) K₂O vs. Na₂O diagram (Chappell & White, 2001)

Owing to the fact that trace elements are immobile during low-grade metamorphism, hydrothermal alteration and weathering, they can be so beneficial to identify the origin of magma and related processes (Rollinson & Pease, 2021). In the chondrite-normalized REE diagram (Boynton, 1984), the rock samples of the Shadan area reveal a relatively parallel trend for REE patterns, which demonstrate the same magmatic processes. According to this diagram, most of the rock samples represent enrichment in Eu, which is related to abundance of plagioclase in Shadan rocks and a negative anomaly in Sm. Generally, there is an apparent enrichment in LREE compared to HREE (Fig. 7a). The primitive mantle-normalized trace elements spider diagram (Sun & McDonough, 1989) indicate enrichment in LILE such as K, Rb and Cs compared to HFSE (Nb, Zr and Ti) (Fig. 7b). Negative P anomalies may be related to fractionation of apatite, while negative Nb and Ti anomalies is widely attributed to Ti-bearing phases fractionation (titanite, amphibole etc.) and distinctive features of crustal contamination and/or arc crust (Rollinson, 1993).

Harker diagrams of variation of major oxides versus SiO₂ can play a key role in interpreting geochemical attributes of magma (Harker, 1909). K₂O and Na₂O indicate positive correlation with SiO₂, proposing contribution of them in producing K-feldspars and albitic plagioclase (Fig. 8c and e). On the other hand, Al₂O₃, CaO, MgO, P₂O₅, TiO₂ and Fe₂O₃ have negative correlation with SiO₂, which illustrate crystallization Ca-bearing plagioclase, hornblende, clinopyroxene, biotite, iron and titanium oxides and phosphorous minerals (Fig. 8a, b, d, f, g and h).

Geochemical data analysis is a great way to determine magmatic processes such as fractional crystallization, contamination and magma mixing, and petrogenesis of intrusive rocks. The intense Cenozoic volcanic activities in east of Iran is related to the subduction of the Neo-Tethys ocean and its branches (Darvishzadeh, 2004; Pang et al., 2013).

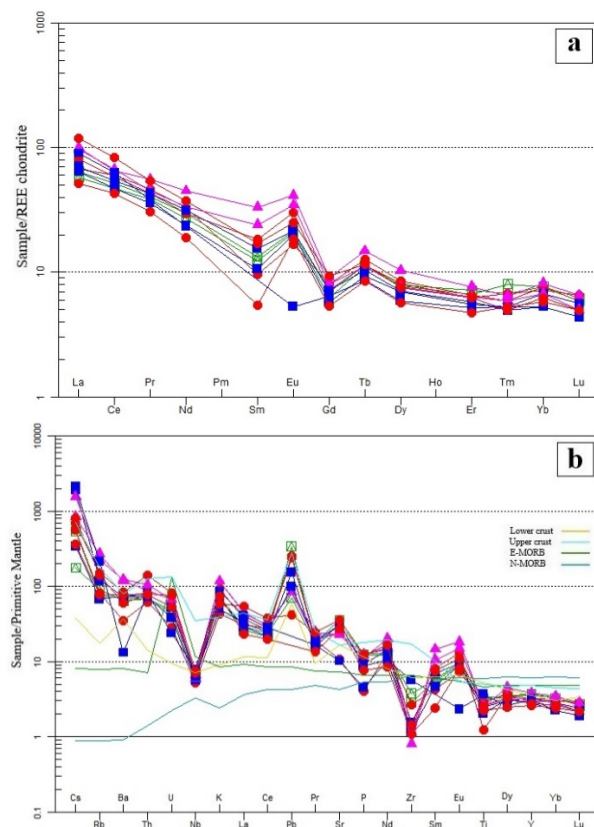


Figure 7. a) Chondrite-normalized REE patterns (Boynton, 1984); b) Primitive mantle-normalized trace element spider diagram (Sun & McDonough, 1989). Lower crust and upper crust data from (Rudnick & Fountain, 1995). E-MORB and N-MORB data from (Sun & McDonough, 1989)

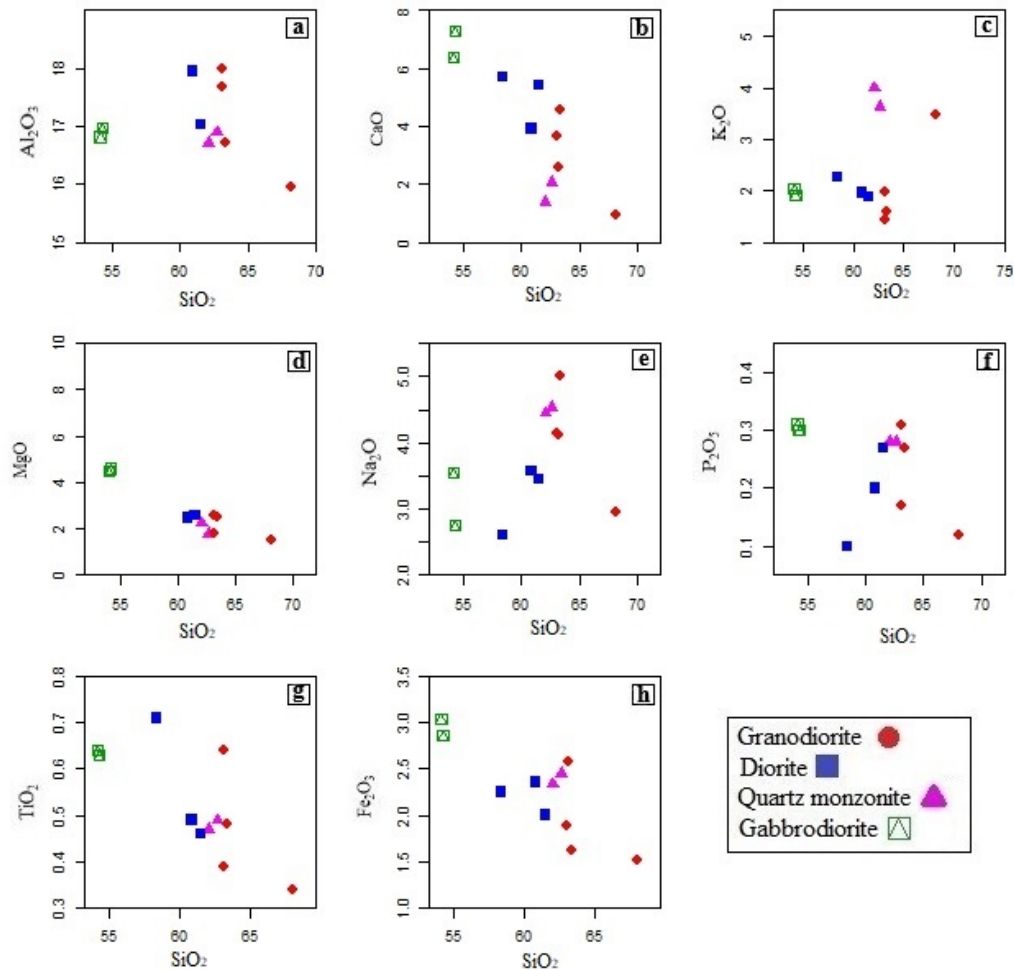


Figure 8. Plots of silica contents vs. major oxides of Shadan rock samples a) Al_2O_3 , b) CaO , c) K_2O , d) MgO , e) Na_2O , f) P_2O_5 , g) TiO_2 , h) Fe_2O_3 (Harker, 1909)

Also based on the geochronological and geochemical studies of the Lut block igneous rocks, most of the magmatism occurred during the Middle Eocene (Tarkian et al., 1983; Malekzadeh et al., 2010; Karimpour et al., 2011). According to these studies and the age of the Shadan area (Late Eocene), Shadan magmatic processes are related to the subduction of the Neo-Tethys. Nb/Y vs. Rb/Y diagram (Temel et al., 1998) shows crustal contamination associated with the subduction zone enrichment (Fig. 9a). Based on Nb/Ba vs. Nb/Zr diagram (Hooper & Hawkesworth, 1993), Shadan intrusive rocks are related to the subcontinental lithosphere (Fig. 9b). According to Th/Yb versus Nb/Yb diagram (Pearce, 2008), Shadan samples and MORB-OIB arrays separated (Fig. 9c), which may be due to crustal contamination (Zhao et al., 2013; Dai et al., 2015; Liu et al., 2016). Pearce (2008) states that magma-crust interaction and mobility of Th during subduction explain why rock samples are displaced above the MORB-OIB arrays. He also argues that even without involvement of contamination, the presence of subcontinental lithosphere can play a significant role in the mobility of Th. La vs. La/Yb diagram (Fig. 9d) displays partial melting in the formation of Shadan intrusive and subvolcanic rocks (Wang et al., 2007).

Based on Th vs. Ta (Fig. 10a) and Th/Hf vs. Ta/Hf (Fig. 10b) diagrams (Schandl & Gorton, 2002), all the Shadan rock samples are plotted in active continental margins. According to Nb vs. Y (Fig. 11a) and Rb vs. Ta+Yb (Fig. 11b) diagrams (Pearce et al., 1984), all rock samples of Shadan area fall in the volcanic arc and syncollisional granitoid fields.

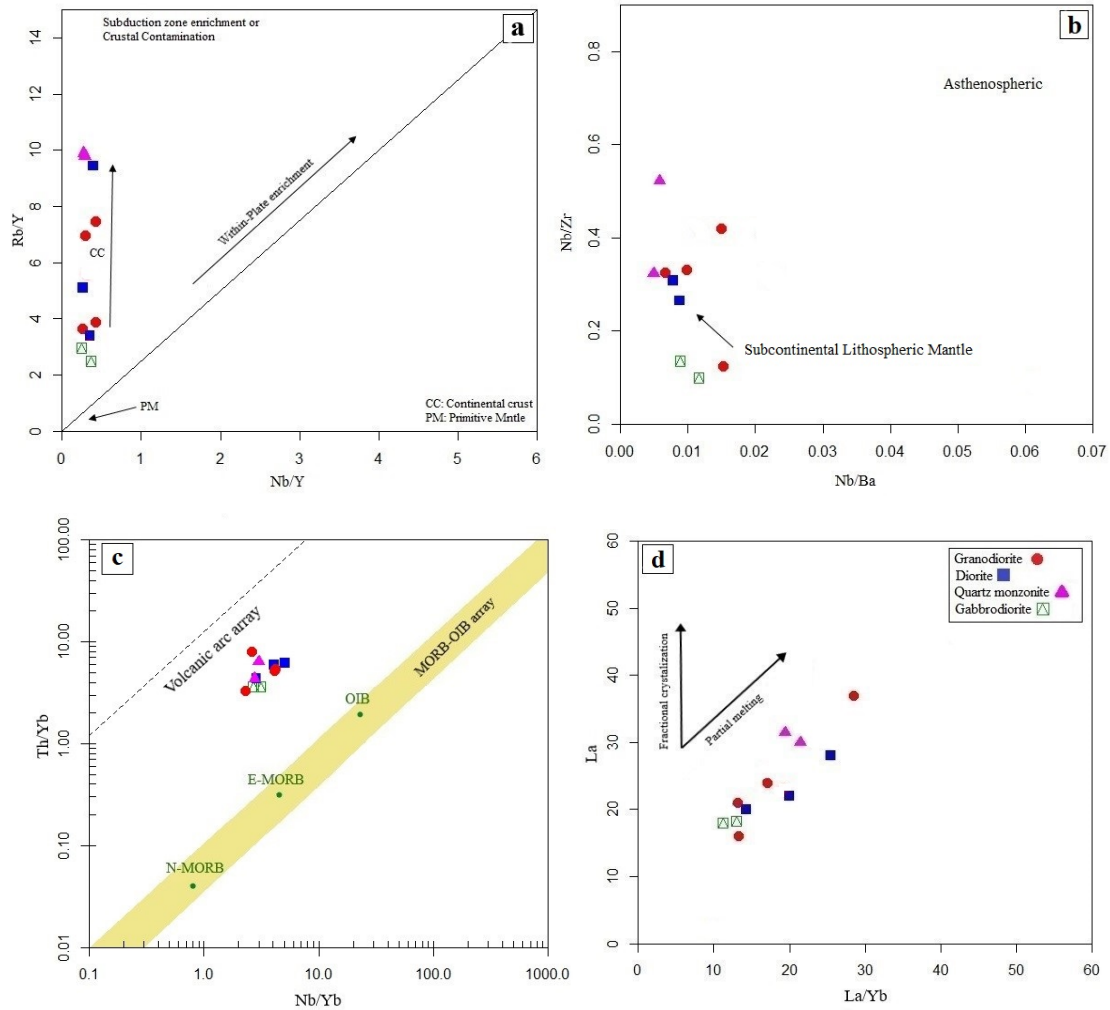


Figure 9. Shadan rock samples plotted on a) Nb/Y vs. Rb/Y diagram (Temel et al., 1998); b) Nb/Ba vs. Nb/Zr diagram (Hooper & Hawkesworth, 1993); c) Th/Yb vs. Nb/Yb diagram (Pearce, 2008); d) Plot of La vs. La/Yb ratio (Wang et al., 2007)

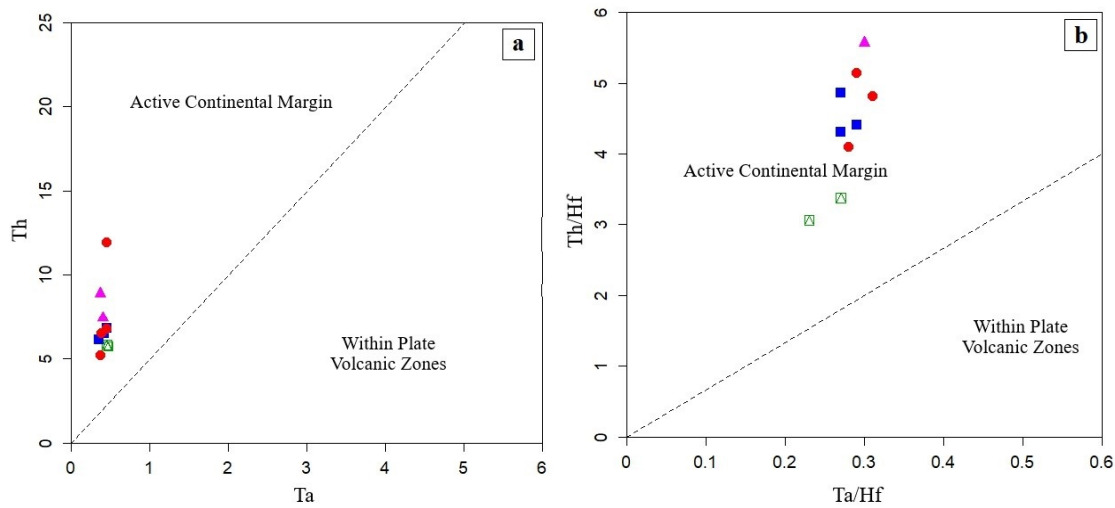


Figure 10. Tectonomagmatic discrimination diagram for Shadan rock samples (Schandl & Gorton, 2002)

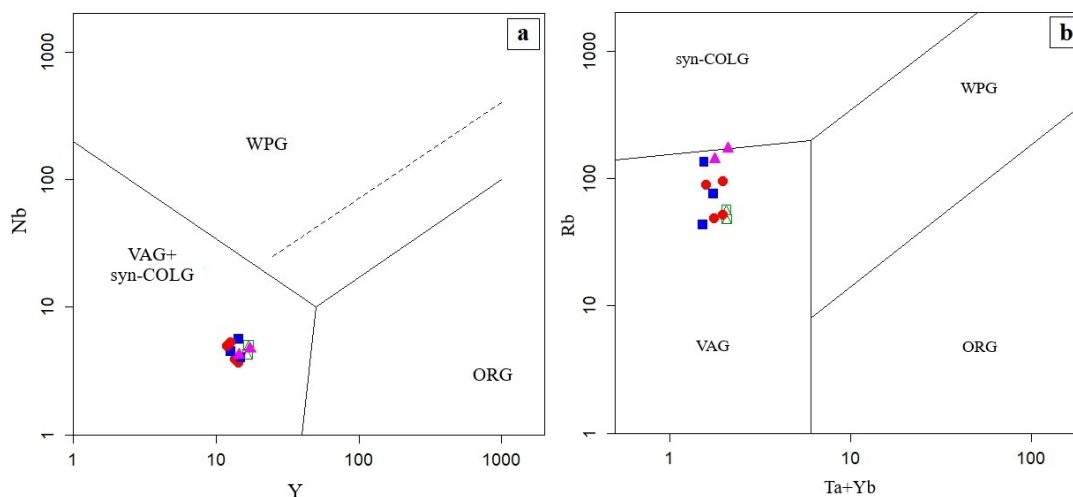


Figure 11. Tectonomagmatic discrimination diagrams for Shadan rocks (Pearce et al., 1984), WPG: within plate granitoids; VAG: volcanic arc granitoids; ORG: ocean ridge granitoids; syn-COLG: syncollisional granitoids

Conclusion

Geochemical and petrographic studies indicated that the Shadan intrusive and subvolcanic rocks are intermediate to felsic in composition, and calc-alkaline to high-potassic calc-alkaline in nature. These rocks are I-type, metaluminous to peraluminous and comprise granodiorite, quartz monzonite, and diorite to microgabbrodiorite. Geochemical signatures such as enrichment in LREE and LILE relative to HREE and HFSE show a subduction zone in an active continental margin setting. According to petrographic studies, porphyroid is the main texture of these rocks and their phenocrysts include plagioclase, quartz, K-feldspar, hornblende, and magmatic biotite. Quartz-carbonate, propylitic, argillic, phyllic and potassic are the main hydrothermal alteration zones in the study area. Based on this study, Shadan rocks originated from the subcontinental lithospheric mantle. They have shown subduction zone enrichment and crustal contamination. There is a separation between Shadan samples and MORB-OIB arrays in the Th/Yb and Nb/Yb diagrams, which may be caused by crustal contamination and the mobility of Th during subduction. In addition, partial melting is an undivided process during formation Shadan intrusive and subvolcanic rocks.

Acknowledgements

The authors would like to express their highest gratitude to directors and senior experts of the Karand Sadr-e-Jahan Company for their help and financial support of this work.

References

- Arjmandzadeh, R., Karimpour, M.H., Mazaheri, S.A., Santos, J.F., Medina, J.M., Homam, S.M., 2011. Two-sided asymmetric subduction; implications for tectonomagmatic and metallogenic evolution of the Lut Block, eastern Iran. *Journal of Economic Geology* 1(3): 1-14.
- Askren, D.R., Roden, M.F., Whitney, J.A., 1997. Petrogenesis of Tertiary andesite lava flows interlayered with large-volume felsic ash-flow tuffs of the western USA. *Journal of Petrology* 38(8): 1021-1046.
- Berberian, M., King, G.C.P., 1981. Towards a paleogeography and tectonic evolution of Iran. *Canadian journal of earth sciences* 18(2): 210-265.
- Boynton, W.V., 1984. Cosmochemistry of the rare earth elements: meteorite studies. In *Developments*

- in geochemistry 2:63-114.
- Camp, V.E., Griffis, R.J., 1982. Character, genesis and tectonic setting of igneous rocks in the Sistan suture zone, eastern Iran. *Lithos* 15(3): 221-239.
- Chappell, B.W., White, A.J., 2001. Two contrasting granite types: 25 years later. *Australian journal of earth sciences* 48(4): 489-499.
- Dai, L.Q., Zhao, Z.F., Zheng, Y.F. and Zhang, J., 2015. Source and magma mixing processes in continental subduction factory: Geochemical evidence from postcollisional mafic igneous rocks in the Dabie orogen. *Geochemistry, Geophysics, Geosystems*, 16(3), pp.659-680.
- Darvishzadeh, A., 2004. *Geology of Iran: stratigraphy, tectonic, metamorphism, and magmatism*. Amir kabir, Tehran.
- Harker, A., 1909. *The natural history of igneous rocks*. Methuen and Company, London, 344p
- Hooper, P.R., Hawkesworth, C.J., 1993. Isotopic and geochemical constraints on the origin and evolution of the Columbia River Basalt. *Journal of Petrology* 34(6): 1203-1246. h
- Karimpour, M.H., Malekzadeh, A., Hidareian, M.R. and Askari, A., 2007. Mineralization, alteration and geochemistry of Hired gold-tin prospecting area, South Khorasan province. *Iran. J. Crystallogr. Miner.*, 15(1), pp.67-90.
- Karimpour, M.H., Stern, C., Farmer, L., Saadat, S., 2011. Review of age, Rb-Sr geochemistry and petrogenesis of Jurassic to Quaternary igneous rocks in Lut Block, Eastern Iran. *Geopersia* 1(1): 19-54.
- Liu, B., Ma, C.Q., Guo, Y.H., Xiong, F.H., Guo, P. and Zhang, X., 2016. Petrogenesis and tectonic implications of Triassic mafic complexes with MORB/OIB affinities from the western Garzê-Litang ophiolitic mélange, central Tibetan Plateau. *Lithos*, 260: 253-267.
- Mahdavi, P., Jafari Rad, A., Heuss-Abichler, S., Lotfi, M. and Nezafati, N., 2020. Geology, mineralogy, and fluids inclusion studies in Shadan copper-gold deposit, Southern Khorasan. *Geopersia*, 10(2): 263-275.
- Malekzadeh Shafaroudi, A. and Karimpour, M.H., 2011. Zircon U-Pb dating of Maherabad porphyry copper-gold prospect area: evidence for a late Eocene porphyry-related metallogenic epoch in east of Iran. *Journal of Economic Geology*, 3(1): 41-60.
- Malekzadeh, S.A., Karimpour, M.H. and Mazaheri, S.A., 2010. Rb-Sr and Sm-Nd isotopic compositions and Petrogenesis of ore-related intrusive rocks of gold-rich porphyry copper Maherabad prospect area (north of Hanich), east of Iran.
- Modabberi, S., Namayandeh, A., Setti, M., López-Galindo, A., 2019. Genesis of the Eastern Iranian bentonite deposits. *Applied Clay Science* 168: 56-67.
- Omidianfar, S., Monsef, I., Rahgoshay, M., Zheng, J., Cousens, B., 2020. The middle Eocene high-K magmatism in Eastern Iran Magmatic Belt: constraints from U-Pb zircon geochronology and Sr-Nd isotopic ratios. *International Geology Review* 62(13-14): 1751-1768.
- Pang, K.N., Chung, S.L., Zarrinkoub, M.H., Khatib, M.M., Mohammadi, S.S., Chiu, H.Y., Chu, C.H., Lee, H.Y., Lo, C.H., 2013. Eocene-Oligocene post-collisional magmatism in the Lut-Sistan region, eastern Iran: Magma genesis and tectonic implications. *Lithos* 180: 234-251.
- Pearce, J.A., 2008. Geochemical fingerprinting of oceanic basalts with applications to ophiolite classification and the search for Archean oceanic crust. *Lithos* 100(1-4): 14-48.
- Pearce, J.A., Harris, N.B., Tindle, A.G., 1984. Trace element discrimination diagrams for the tectonic interpretation of granitic rocks. *Journal of petrology* 25(4): 956-983.
- Peccerillo, A., Taylor, S.R., 1976. Geochemistry of Eocene calc-alkaline volcanic rocks from the Kastamonu area, northern Turkey. *Contributions to mineralogy and petrology* 58(1): 63-81.
- Richards, J.P., 2015. Tectonic, magmatic, and metallogenic evolution of the Tethyan orogen: From subduction to collision. *Ore Geology Reviews* 70: 323-345.
- Richards, J.P., Sholeh, A., 2016. The Tethyan tectonic history and Cu-Au metallogeny of Iran. *Tectonics and Metallogeny of the Tethyan Orogenic Belt*. Society of Economic Geologists, Special Publication 19: 193-212.
- Richards, J.P., Spell, T., Rameh, E., Raziq, A. and Fletcher, T., 2012. High Sr/Y magmas reflect arc maturity, high magmatic water content, and porphyry Cu±Mo±Au potential: Examples from the Tethyan arcs of central and eastern Iran and western Pakistan. *Economic geology*, 107(2): 295-332.
- Rollinson, H., Pease, V., 2021. *Using Geochemical Data: To Understand Geological Processes*. Cambridge University Press.
- Rollinson, H.R., 1993. *Using Geochemical Data: Evaluation, Presentation, Interpretation*. Longman

- Scientific and Technical, London, p. 352.
- Rudnick, R.L., Fountain, D.M., 1995. Nature and composition of the continental crust: a lower crustal perspective. *Reviews of geophysics* 33(3): 267-309.
- Saccani, E., Delavari, M., Beccaluva, L., Amini, S., 2010. Petrological and geochemical constraints on the origin of the Nehbandan ophiolitic complex (eastern Iran): Implication for the evolution of the Sistan Ocean. *Lithos* 117(1-4): 209-228.
- Samiee, S., Ghaderi, M. and Zirjanizadeh, S., 2019. Geochemistry, Fluid Inclusion and Sulfur Isotopes Studies of Hydrothermal Breccia Gold Mineralization in the Khunik Area, Khorasan Jonoubi Province (Iran). *Journal of Economic Geology*, 11(3): 473-495.
- Schandl, E.S., Gorton, M.P., 2002. Application of high field strength elements to discriminate tectonic settings in VMS environments. *Economic geology* 97(3): 629-642.
- Shafaroudi, A.M., Karimpour, M.H. and Stern, C.R., 2015. The Khopik porphyry copper prospect, Lut Block, Eastern Iran: geology, alteration and mineralization, fluid inclusion, and oxygen isotope studies. *Ore Geology Reviews*, 65: 522-544.
- Stöcklin, J., 1968. Structural history and tectonics of Iran: a review. *AAPG bulletin* 52(7): 1229-1258.
- Sun, S.S., McDonough, W.F., 1989. Chemical and isotopic systematics of oceanic basalts: implications for mantle composition and processes. *Geological Society, London, Special Publications* 42(1): 313-345.
- Tarkian, M., Lotfi, M., & Baumann, A., 1983. Tectonic, magmatism and the formation of mineral deposits in the central Lut, east Iran.
- Temel, A., Gündoğdu, M.N., Gourgaud, A., 1998. Petrological and geochemical characteristics of Cenozoic high-K calc-alkaline volcanism in Konya, Central Anatolia, Turkey. *Journal of volcanology and geothermal research* 85(1-4): 327-354.
- Tirrul, R., Bell, I.R., Griffis, R.J., Camp, V.E., 1983. The Sistan suture zone of eastern Iran. *Geological Society of America Bulletin* 94(1): 134-150.
- Vahdati-Daneshmand, F., Eftekhari-Nezhad, J., 1991. Geological map of Birjand Scale 1:250000. Geological Survey of Iran.
- Vassigh, H., Soheili, M., 1975. Geological map of Sar-E-chah-E-Shur Scale 1:100000. Geological Survey of Iran.
- Verdel, C., Wernicke, B.P., Hassanzadeh, J., Guest, B., 2011. A Paleogene extensional arc flare-up in Iran. *Tectonics* 30(3).
- Wang, Q., Wyman, D.A., Xu, J., Jian, P., Zhao, Z., Li, C., Xu, W., Ma, J., He, B., 2007. Early Cretaceous adakitic granites in the Northern Dabie Complex, central China: implications for partial melting and delamination of thickened lower crust. *Geochimica et cosmochimica acta* 71(10): 2609-2636.
- Zarrinkoub, M.H., Pang, K.N., Chung, S.L., Khatib, M.M., Mohammadi, S.S., Chiu, H.Y., Lee, H.Y., 2012. Zircon U–Pb age and geochemical constraints on the origin of the Birjand ophiolite, Sistan suture zone, eastern Iran. *Lithos* 154: 392-405.
- Zhao, Z.F., Dai, L.Q. and Zheng, Y.F., 2013. Postcollisional mafic igneous rocks record crust-mantle interaction during continental deep subduction. *Scientific Reports*, 3(1): 1-6.

